Continuum centroid classifier for functional data

Zhiyang Zhou<sup>1</sup> and Peijun Sang<sup>2\*</sup>

<sup>1</sup>Department of Preventive Medicine, Northwestern University Feinberg School of Medicine,

Chicago, IL 60611, United States

<sup>2</sup>Department of Statistics & Actuarial Science, University of Waterloo, ON N2L 3G1, Canada

Key words and phrases: Centroid classifier; Continuum regression; Functional linear model;

Functional partial least square; Functional principal component.

MSC 2010: Primary 62G08; secondary 62H30

Abstract: Aiming at the binary classification of functional data, we propose the continuum cen-

troid classifier (CCC) built upon projections of functional data onto one specific direction. This

direction is obtained via bridging the regression and classification. Controlling the extent of su-

pervision, our technique is neither unsupervised nor fully supervised. Thanks to the intrinsic

infinite dimension of functional data, one of two subtypes of CCC enjoys the (asymptotic) zero

misclassification rate. Our proposal includes an effective algorithm that yields a consistent em-

pirical counterpart of CCC. Simulation studies demonstrate the performance of CCC in different

scenarios. Finally, we apply CCC to two real examples. The Canadian Journal of Statistics xx: 1-

25; 2021 © 2021 Statistical Society of Canada

\* Author to whom correspondence may be addressed.

E-mail: peijun.sang@uwaterloo.ca

*Résumé:* Insérer votre résumé ici. We will supply a French abstract for those authors who can't prepare it themselves. *La revue canadienne de statistique* xx: 1–25; 2021 © 2021 Société statistique du Canada

#### 1. INTRODUCTION

With the development of technology, data with complex structures such as curves and images have become more and more popular in various fields. Functional data analysis (FDA) handles one type of such data, which take values over a continuum like space or time. Typical examples of functional data include intraday yield curves for high frequency trading, near-infrared spectra and blood signals measured in functional magnetic resonance imaging. For a comprehensive overview of FDA, one can refer to, e.g. Ramsay and Silverman (2005) and Ferraty and Vieu (2006).

One important problem in FDA is the classification for functional data, which is potentially applicable to, for instance, the diagnosis of multiple sclerosis (MS). MS is an immune disorder which impairs the central nervous system. Typical symptoms of MS include fatigue, vision problems, sensation impairment and cognitive impairment. Traditionally the diagnosis of MS relies on signs, symptoms and medical tests; yet, as reported by Sbardella et al. (2013), some important results in MS study have been obtained from applications of diffusion tensor imaging (DTI), since DTI is a powerful tool in quantifying the demyelination and axonal loss resulted from MS (Goldsmith et al., 2012). If DTI results are

recorded for both healthy controls and MS patients, the corresponding diagnosis can be interpreted as classifying curves into two status, i.e. a binary functional classification problem. More details about this application will be presented in Section 3.

In the literature of FDA, there has been extensive research on functional data classification. Ferraty and Vieu (2003) proposed a kernel estimator of the posterior probability that a new curve belongs to a given class. Shin (2008) extended the linear discriminant analysis (LDA) to functional data. The former work defines a distance between curves, while the latter one makes use of the reproducing kernel Hilbert space to define an inner product; both of them are built upon the infinite dimensional space where functional data lie. As pointed out by Fan et al. (2012), a large number of covariates would pose challenges for classification in the multivariate context. Functional data, however, are intrinsically infinite dimensional. In light of this fact, many researchers suggest reducing the dimension first and then implementing classification algorithms in the reduced space. Functional principal component (FPC) analysis is one of the most commonly used approaches for dimension reduction. Projections of functional data onto the directions of functional principal components are referred to as FPC scores in the literature. Galeano et al. (2015) proposed both linear and quadratic Bayes classifiers on FPC scores. Dai et al. (2017) further extended this idea to density ratios of FPC scores and showed that the resulting classifier is equivalent to the quadratic discriminant analysis (QDA) for Gaussian random curves. Additionally, a logistic regression on FPC scores was considered in Leng and Müller (2005) to discriminate temporal gene regulation data. Rossi and Villa (2006) implemented the support vector machine on FPC scores.

Our work is mainly motivated by the centroid classifier proposed by Delaigle and Hall (2012) who suggested projecting functional data to a specific direction first. To identify this projection direction, the authors converted the classification problem to a functional linear regression problem. The slope function in the functional linear model is then taken as the projection direction they needed. They proposed two methods in estimating the slope function: one with FPC basis functions and the other with the functional partial least squares (FPLS) basis functions. The first method accounts for the variability of functional covariates but ignores the information of the outcome when estimating the projection direction, whereas the second one focuses on the covariance between the outcome and the functional covariate. As argued in Jung (2018), the projection direction from FPC basis sometimes fails to capture the difference between mean functions, while FPLS basis is prone to sensitivity and vulnerability to small signals; a combination of these two ideas may be preferable than either of them. We therefore propose a new method to estimate the projection direction, which captures both variability of functional data and covariance between the functional covariate and the outcome. A distance-based centroid classifier is then provided after

projecting functional data onto this specific direction. Moreover, under some regularity conditions, we establish the asymptotic perfect classification property for the newly proposed classifier. Both simulation studies and real examples demonstrate that our proposed classifier compares favorably with the two methods given by Delaigle and Hall (2012) in terms of classification accuracy in finite samples.

The rest of this paper is organized as follows. In Section 2, we introduce the two subtypes of our classifier, including both the population and empirical versions, and then establish the property of (asymptotically) perfect classification. The numerical illustration in Section 3 investigates the performance of our proposal, highlighting the settings in favor of it. Section 4 gives concluding remarks as well as discussions. Technical details are relegated to Appendix.

#### 2. METHODOLOGY AND THEORY

### 2.1. Formalization of the problem

Suppose that  $(X_1, Y_1), \ldots, (X_N, Y_N)$  are n independently and identically distributed (iid) copies of (X, Y), where X is a random function defined on the interval  $\mathcal{T} = [t_{\min}, t_{\max}]$ , and Y is the label of X taking values 0 or 1. In other words, each  $X_i$  is sampled from a mixture of two populations  $\Pi_0$  and  $\Pi_1$  with the indicator  $Y_i = \mathbb{1}(X_i \in \Pi_1)$ . Of interest is the binary classification for a newly observed  $X^*$  distributed as X but independent of  $X_1, \ldots, X_N$ . Assume that the sub-mean and sub-covariance functions for  $\Pi_k$ , k = 0, 1, are respectively

$$\mu_{[k]}(t) = \mathrm{E}\{X(t) \mid Y = k\}$$
 (1)

and, for all  $s, t \in \mathcal{T}$ ,

$$v_X^{[k]}(s,t) = \text{cov}\{X(s), X(t) \mid Y = k\}.$$
(2)

Let  $\pi_0 = \Pr(X_i \in \Pi_0) \in (0,1)$ . We have decomposition

$$\mu(\cdot) = E X(\cdot) = \pi_0 \mu_{[0]}(\cdot) + (1 - \pi_0) \mu_{[1]}(\cdot)$$

as well as, according to the law of total covariance,

$$v_X(s,t) = \text{cov}\{X(s), X(t)\} = v_X^W(s,t) + v_X^B(s,t),$$
(3)

where

$$v_X^W(s,t) = \pi_0 v_X^{[0]}(s,t) + (1-\pi_0) v_X^{[1]}(s,t), \tag{4}$$

$$v_X^B(s,t) = \pi_0(1-\pi_0)\{\mu_{[1]}(s) - \mu_{[0]}(s)\}\{\mu_{[1]}(t) - \mu_{[0]}(t)\}$$

are respectively the within- and between-group covariance functions. Correspondingly, define covariance operators  $\mathcal{V}_X, \mathcal{V}_X^{[k]}: L^2(\mathcal{T}) \to L^2(\mathcal{T}), \ k=0,1,$  such that, for  $f \in L^2(\mathcal{T})$ ,

$$\mathcal{V}_X(f)(\cdot) = \int_{\mathcal{T}} f(s) v_X(s, \cdot) \, \mathrm{d}s,$$

$$\mathcal{V}_X^{[k]}(f)(\cdot) = \int_{\mathcal{T}} f(s) v_X^{[k]}(s, \cdot) \, \mathrm{d}s.$$

Throughout this paper, we abbreviate the Lebesgue integral  $\int_{\mathcal{T}} f(t) dt$  to  $\int_{\mathcal{T}} f$ . The functions involved in this paper are limited to  $L^2(\mathcal{T})$  (or  $L^2(\mathcal{T}^2)$ ), the collection of square integrable functions defined on  $\mathcal{T}$  (or  $\mathcal{T}^2$ ). The square-integrability of  $v_X$  at (3) (resp.  $v_X^{[k]}$  at (2)) implies that it possesses only a count-

able number of nonnegative eigenvalues  $\{\lambda_1,\lambda_2,\ldots\}$  (resp.  $\{\lambda_{k,1},\lambda_{k,2},\ldots\}$ ), with corresponding eigenfunctions  $\{\phi_1,\phi_2,\ldots\}$  (resp.  $\{\phi_{k1},\phi_{k2},\ldots\}$ ), k=0,1. In addition,  $\|\cdot\|$  stands for the  $L^2$ -norm, i.e.,  $\|f\|$  equals  $(\int_{\mathcal{T}} f^2)^{1/2}$  for  $f\in L^2(\mathcal{T})$  and  $(\int_{\mathcal{T}} \int_{\mathcal{T}} f^2)^{1/2}$  if  $f\in L^2(\mathcal{T}^2)$ .

## 2.2. Review of centroid classifier

Before proceeding to our proposal, we first review the centroid classifier proposed by Delaigle and Hall (2012). They projected functional data onto the one-dimensional space spanned by a given function  $\omega \in L^2(\mathcal{T})$ , say  $\mathrm{span}(\omega)$ , and then constructed the classifier with the projection. Specifically, they defined a classifier

$$\mathcal{D}(X^* \mid \omega) = \left\{ \int_{\mathcal{T}} \frac{\omega}{\|\omega\|} (X^* - \mu_{[1]}) \right\}^2 - \left\{ \int_{\mathcal{T}} \frac{\omega}{\|\omega\|} (X^* - \mu_{[0]}) \right\}^2 + 2 \ln \frac{\pi_0}{1 - \pi_0}, \quad (5)$$

where  $|\int_{\mathcal{T}} \omega(X^* - \mu_{[k]})|/||\omega||$ , the magnitude of the projection of  $X^* - \mu_{[k]}$  onto  $\mathrm{span}(\omega)$ , can be regarded as the distance from  $X^*$  to  $\mu_{[k]}$  (1). When  $\mathcal{D}(X^* \mid \omega)$  is positive,  $X^*$  is thought to be closer to  $\mu_{[0]}$  and hence assigned to  $\Pi_0$  and vice versa. Given  $\omega$ , this principle is identical to LDA assuming  $\int_{\mathcal{T}} X\omega$  to be normally distributed conditional on  $X \in \Pi_k$  with  $\mathrm{var}(\int_{\mathcal{T}} X\omega \mid X \in \Pi_k) = ||\omega||^2$  for each k, viz.  $\int_{\mathbb{T}} X\omega \mid X \in \Pi_k \sim \mathcal{N}(\int_{\mathbb{T}} \mu_{[k]}\omega, ||\omega||_2^2)$ .

It remains to select a direction  $\omega \in L^2(\mathcal{T})$  to optimize the misclassification rate

$$\operatorname{err}\{\mathcal{D}(X^* \mid \omega)\} = \pi_0 \Pr\{\mathcal{D}(X^* \mid \omega) < 0 \mid X^* \in \Pi_0\} + (1 - \pi_0) \Pr\{\mathcal{D}(X^* \mid \omega) > 0 \mid X^* \in \Pi_1\}.$$

Delaigle and Hall (2012) proposed taking  $\omega = \beta_{p,\text{FPC}}$  at (6) (resp.  $\beta_{p,\text{FPLS}}$  at (7)), corresponding to FPC (concentrated on  $v_X^W$  at (4)) (resp. FPLS) basis, with a positive integer p tuned via cross-validation. The resulting classifier  $\mathcal{D}(X^* \mid \beta_{p,\text{FPC}})$  (resp.  $\mathcal{D}(X^* \mid \beta_{p,\text{FPLS}})$ ) is abbreviated to be PCC (resp. PLCC). More specifically, these two projection directions are defined as

$$\beta_{p,\text{FPC}} = \underset{\beta \in \text{span}(\phi_1^W, \dots, \phi_p^W)}{\text{arg min}} \operatorname{E} \left\{ Y - \operatorname{E} Y - \int_{\mathcal{T}} \beta(X - \operatorname{E} X) \right\}^2 \tag{6}$$

and

$$\beta_{p,\text{FPLS}} = \underset{\beta \in \text{span}(w_{1,\text{FPLS}},\dots,w_{p,\text{FPLS}})}{\operatorname{arg\,min}} \operatorname{E} \left\{ Y - \operatorname{E} Y - \int_{\mathcal{T}} \beta(X - \operatorname{E} X) \right\}^{2}, \quad (7)$$

where  $\phi_1^W, \ldots, \phi_p^W$  are the first p eigenfunctions of  $v_X^W$  at (4) and  $w_{1,\text{PLS}}, \ldots, w_{p,\text{PLS}}$  are solutions to the following sequential optimization problems: given  $w_{1,\text{FPLS}}, \ldots, w_{j-1,\text{FPLS}}$ , define

$$w_{j,\text{FPLS}} = \underset{w:||w||=1}{\operatorname{arg max}} \operatorname{cov}^{2} \left( Y, \int_{\mathcal{T}} Xw \right)$$

subject to  $\int_{\mathcal{T}} w \mathcal{V}_X(w_{l,\mathrm{FPLS}}) = 0$ ,  $l = 1, \ldots, j-1$ . Minimizers (6) and (7), yet restricted in different linear spaces, are both slope functions of the (constrained) optimal approximations to Y by a linear functional of X. Taking either of them as  $\omega$  in (5), Delaigle and Hall (2012) succeeded in bridging the binary classification

problem to the functional linear regression.

#### 2.3. Continuum centroid classifier

As mentioned in Section 1, an intermediate state between FPC and FPLS bases may be preferred. Fixing  $\alpha \in [0, 1)$ , Zhou (2019, Proposition 4) defined the functional continuum (FC) basis functions as sequential constrained maximizers of

$$T_{j,\alpha}(w) = \cos^2\left(Y^{[j,\alpha]}, \int_{\mathcal{T}} X^{[j,\alpha]}w\right) \cdot \operatorname{var}^{-1 + \frac{\alpha}{1-\alpha}}\left(\int_{\mathcal{T}} X^{[j,\alpha]}w\right), \quad (8)$$

where

$$X^{[j,\alpha]} = X^{[j-1,\alpha]} - \text{var}^{-1/2} \left( \int_{\mathcal{T}} X w_{j-1,\alpha} \right) \cdot \left( \int_{\mathcal{T}} X^{[1,\alpha]} w_{j-1,\alpha} \right) \cdot \mathcal{V}_X \left( w_{j-1,\alpha} \right),$$

and, for j = 2, 3, ...,

$$Y^{[j,\alpha]} = Y^{[j-1,\alpha]} - EY - \int_{\mathcal{T}} X^{[1,\alpha]} \beta_{j-1,\alpha},$$

with  $X^{[1,\alpha]}=X-\operatorname{E} X$  and  $Y^{[1,\alpha]}=Y-\operatorname{E} Y.$  Specifically, given  $w_{1,\alpha},\dots,w_{j-1,\alpha}$ , the jth FC basis function is

$$w_{j,\alpha} = \underset{w:||w||=1}{\arg\max} \ T_{j,\alpha}(w). \tag{9}$$

FC basis captures not only variation of X but also the covariance between X and Y; thus this dimension reduction technique lies midway between (unsupervised) FPC and (fully supervised) FPLS. FC basis reduces to FPLS when  $\alpha=1/2$  and becomes irrelevant to Y as  $\alpha$  diverges. By tuning  $\alpha$ , FC basis controls the extent of supervision and is expected to be neither unsupervised nor too supervised.

The continuum centroid classifier (CCC) is defined by substituting

$$\beta_{p,\alpha} = \underset{\beta \in \operatorname{span}(w_{1,\alpha},\dots,w_{p,\alpha})}{\operatorname{arg\,min}} \operatorname{E} \left\{ Y - \operatorname{E} Y - \int_{\mathcal{T}} \beta(X - \operatorname{E} X) \right\}^{2}$$
 (10)

for  $\omega$  in (5) and, simultaneously, dropping the assumption  $\operatorname{var}(\int_{\mathcal{T}} X\omega \mid X \in \Pi_k) = \|\omega\|^2$ . In details, CCC assigns a label to a random trajectory  $X^*$  by respectively applying LDA and QDA to  $\int_{\mathcal{T}} X^* \beta_{p,\alpha}$  and hence owns two subtypes, say CCC-L and CCC-Q: CCC-Q is given by

$$\mathcal{D}_{Q}(X^{*} \mid \beta_{p,\alpha}) = \sigma_{[1]}^{-2}(\beta_{p,\alpha}) \left\{ \int_{\mathcal{T}} \beta_{p,\alpha}(X^{*} - \mu_{[1]}) \right\}^{2}$$
$$- \sigma_{[0]}^{-2}(\beta_{p,\alpha}) \left\{ \int_{\mathcal{T}} \beta_{p,\alpha}(X^{*} - \mu_{[0]}) \right\}^{2} + 2 \ln \frac{\pi_{0}\sigma_{[1]}(\beta_{p,\alpha})}{(1 - \pi_{0})\sigma_{[0]}(\beta_{p,\alpha})}$$
(11)

with

$$\sigma_{[k]}^2(\omega) = \operatorname{var}\left(\int_{\mathcal{T}} X\omega \mid X \in \Pi_k\right) \tag{12}$$

for each k, and CCC-L by

$$\mathcal{D}_{L}(X^{*} \mid \beta_{p,\alpha}) = \left\{ \int_{\mathcal{T}} \beta_{p,\alpha}(X^{*} - \mu_{[1]}) \right\}^{2} - \left\{ \int_{\mathcal{T}} \beta_{p,\alpha}(X^{*} - \mu_{[0]}) \right\}^{2} + 2\sigma^{2}(\beta_{p,\alpha}) \ln \frac{\pi_{0}}{1 - \pi_{0}}$$
(13)

if one believes  $\sigma^2(\omega) = \sigma^2_{[0]}(\omega) = \sigma^2_{[1]}(\omega)$ . Analogous to (5), positive  $\mathcal{D}_L(X^* \mid \beta_{p,\alpha})$  (or  $\mathcal{D}_Q(X^* \mid \beta_{p,\alpha})$ ) suggests classifying  $X^*$  to  $\Pi_0$ .

As long as (C1) in the appendix stands, in theory one can expect an asymptotically perfect classification given by CCC-L; see Proposition 1. It is worth emphasizing that Proposition 1 does not require normality or specific variance

structure of the two sub-populations.

**Proposition 1** Holding (C1), CCC-L asymptotically leads to no misclassification as  $p \to \infty$ .

# 2.3.1. Empirical implementation

In general it is impossible to observe entire trajectories. In this sense, the procedure of estimating  $\beta_{p,\alpha}$  (10) in Zhou (2019) is not detailed enough: the algorithm over there is not described in the matrix form. We fix it in this section.

For brevity,  $X_i$ 's are all assumed to be densely digitized on equispaced M+1 time points  $t_m = t_{\min} + (m-1)\Delta t$ ,  $m=1,\ldots,M+1$ , with  $\Delta t = (t_{\max} - t_{\min})/M$ . Reformulating the infinite-dimensional optimization problem (9) to a finite-dimensional one, we employ the penalized cubic B-spline smoothing (Ramsay and Silverman, 2005, Sections 5.2.4–5.2.5) to each trajectory, i.e., seeking for a surrogate of  $X_i$  in the L (= M+3, as recommended by Ramsay and Silverman, 2005, pp. 86) dimensional linear space

$$BS_L = \operatorname{span}(\psi_1, \dots, \psi_L) \tag{14}$$

spanned by cubic B-splines  $\psi_1, \dots, \psi_L$ ; refer to, e.g., de Boor (2001, Chapter 4), for more details on B-splines. Specifically, the estimator for the *i*th trajectory,  $i = 1, \dots, N$ , is

$$\hat{X}_i = \hat{\boldsymbol{c}}_i^{\mathsf{T}} \boldsymbol{\psi},\tag{15}$$

where

$$\boldsymbol{\psi} = \boldsymbol{\psi}(\cdot) = [\psi_1(\cdot), \dots, \psi_L(\cdot)]^\top, \tag{16}$$

$$\hat{\boldsymbol{c}}_i = (\boldsymbol{\Psi}^\top \boldsymbol{\Psi} + \theta_0 \mathbf{Pen})^{-1} \boldsymbol{\Psi}^\top \boldsymbol{X}_i, \tag{17}$$

with

$$\mathbf{\Psi} = [\psi_k(t_m)]_{(M+1)\times L} = [\boldsymbol{\psi}(t_1), \dots, \boldsymbol{\psi}(t_{M+1})]^\top, \tag{18}$$

$$\mathbf{Pen} = \left[ \int_{\mathcal{T}} \psi_{l_1}'' \psi_{l_2}'' \right]_{1 \le l_1, l_2 \le L},\tag{19}$$

$$X_i = [X_i(t_1), \dots, X_i(t_{M+1})]^{\top}.$$

Positive smoothing parameter  $\theta_0$  is communal for all i and picked up automatically through the generalized cross-validation (GCV, Craven and Wahba, 1979), i.e.,

$$\theta_0 = \arg\min_{\theta} \frac{\sum_{i=1}^{N} \sum_{m=1}^{M+1} \{X_i(t_m) - \hat{X}_i(t_m)\}^2}{[M+1 - \text{trace}\{\Psi(\Psi^{\top}\Psi + \theta \mathbf{Pen})^{-1}\Psi^{\top}\}]^2}.$$

Thanks to dense observations, the presmoothing is able to recover underlying curves accurately (in the  $L^2$  sense) under some regularity conditions. Also, presmoothed curves are anticipated to enhance the classification accuracy (Dai et al., 2017).

**Proposition 2** Holding (C2) and (C3) in the appendix, for each i,  $||\hat{X}_i - X_i|| \to 0$  in probability as  $M \to \infty$ .

The empirical version of  $T_{j,\alpha}$  (8), say  $\hat{T}_{j,\alpha}$ , is then constructed by replacing  $X_i$ ,  $var(\cdot)$ , and  $cov(\cdot)$  in (8) with respective empirical counterparts or, identically, substituting  $\hat{X}_i$  (15) for  $X_i$  in Zhou (2019, Proposition 5).

**Proposition 3** Suppose  $\hat{w}_{j,\alpha} = \max_{w:||w||=1} \hat{T}_{j,\alpha}(w)$  is an estimator of  $w_{j,\alpha}$  (9). Then  $\hat{w}_{j,\alpha}$  must lie in the linear space  $BS_L$ .

Start with optimizing  $\hat{T}_{1,\alpha}(w)$ . Proposition 3 narrows down our search from  $\{w:\|w\|=1, w\in L^2(\mathcal{T})\}$  to  $\{w:w=\boldsymbol{b}^\top\boldsymbol{\psi},\boldsymbol{b}^\top\mathbf{W}\boldsymbol{b}=1,\boldsymbol{b}\in\mathbb{R}^{L\times 1}\}=\{w:w=\boldsymbol{b}^\top\mathbf{W}^{-1/2}\boldsymbol{\psi},\boldsymbol{b}^\top\boldsymbol{b}=1,\boldsymbol{b}\in\mathbb{R}^{L\times 1}\}$  with invertible and symmetric

$$\mathbf{W} = \left[ \int_{\mathcal{T}} \psi_{l_1} \psi_{l_2} \right]_{1 \le l_1, l_2 \le L}.$$
 (20)

The maximization of  $\hat{T}_{1,\alpha}(w)$  (subject to  $\|w\|=1$ ) is reformulated as L-dimensional optimization problem

$$\max_{\boldsymbol{b} \in \mathbb{R}^{L \times 1}} (\boldsymbol{b}^{\top} \mathbf{W}^{1/2} \hat{\mathbf{C}}_{c}^{\top} \boldsymbol{Y}_{c})^{2} (\boldsymbol{b}^{\top} \mathbf{W}^{1/2} \hat{\mathbf{C}}_{c}^{\top} \hat{\mathbf{C}}_{c} \mathbf{W}^{1/2} \boldsymbol{b})^{\alpha/(1-\alpha)-1}$$
(21)

subject to  $\boldsymbol{b}^{\top}\boldsymbol{b}=1$ , where, with  $\hat{\boldsymbol{c}}_i$  at (17),

$$\hat{\mathbf{C}}_{\mathrm{c}} = \left[\hat{oldsymbol{c}}_{1} - \frac{1}{N}\sum_{i=1}^{N}\hat{oldsymbol{c}}_{i}, \ldots, \hat{oldsymbol{c}}_{N} - \frac{1}{N}\sum_{i=1}^{N}\hat{oldsymbol{c}}_{i}\right]^{\top},$$
 $oldsymbol{Y}_{\mathrm{c}} = \left[Y_{1} - \frac{1}{N}\sum_{i=1}^{N}Y_{i}, \ldots, Y_{N} - \frac{1}{N}\sum_{i=1}^{N}Y_{i}\right]^{\top}.$ 

Note that the solution to (21) is necessarily located in the row space of  $\hat{\mathbf{C}}_c \mathbf{W}^{1/2}$ , i.e., the search region is further restricted to  $\{w: w = \boldsymbol{b}^\top \mathbf{V}^\top \mathbf{W}^{-1/2} \boldsymbol{\psi}, \boldsymbol{b}^\top \boldsymbol{b} = 1, \boldsymbol{b} \in \mathbb{R}^{r \times 1}\}$ , where  $r = \operatorname{rank}(\hat{\mathbf{C}}_c \mathbf{W}^{1/2}) \leq \min\{L, N\}$  and  $L \times r$  matrix  $\mathbf{V}$ 

comes from the thin singular value decomposition of  $\hat{\mathbf{C}}_c \mathbf{W}^{1/2}$ :  $\hat{\mathbf{C}}_c \mathbf{W}^{1/2}$  is decomposed into  $\mathbf{U}\mathbf{R}\mathbf{V}^{\top}$  with an invertible diagonal matrix  $\mathbf{R}$  and semi-orthogonal matrices  $\mathbf{U}$  and  $\mathbf{V}$  such that  $\mathbf{U}^{\top}\mathbf{U} = \mathbf{V}^{\top}\mathbf{V} = \mathbf{I}_r$ . In this way the dimension of (21) is further reduced to r.

Write  $\mathbf{G}_1 = \mathbf{U}\mathbf{R}$ . The estimator of the first FC basis function then takes the form

$$\hat{w}_{1,lpha} = oldsymbol{b}_{1,lpha}^ op \mathbf{V}^ op \mathbf{W}^{-1/2} oldsymbol{\psi}$$

in which

$$oldsymbol{b}_{1,lpha} = rgmax_{oldsymbol{b}\in\mathbb{R}^{r imes1},oldsymbol{b}^{ op}oldsymbol{b}=1} (oldsymbol{b}^{ op}oldsymbol{G}_1^{ op}oldsymbol{Y}_{c})^2 (oldsymbol{b}^{ op}oldsymbol{G}_1^{ op}oldsymbol{G}_1)^{lpha/(1-lpha)-1}.$$

Subsequently and successively, for  $j \geq 2$ , given j-1 vectors  $\boldsymbol{b}_{1,\alpha},\dots,\boldsymbol{b}_{j-1,\alpha}$ , we just have to replace previous  $\mathbf{G}_1$  with deflated  $\mathbf{G}_j = \mathbf{P}_{j-1}\mathbf{G}_1$ , where  $\mathbf{P}_0 = \mathbf{I}_N$  and  $\mathbf{P}_{j-1} = \mathbf{I}_N - \mathbf{H}_{j-1}(\mathbf{H}_{j-1}^{\top}\mathbf{H}_{j-1})^{-1}\mathbf{H}_{j-1}^{\top}$  is the projection matrix associated with the orthogonal complement of column space of

$$\mathbf{H}_{i-1} = \hat{\mathbf{C}}_{\mathrm{c}} \mathbf{W}^{1/2} [\mathbf{V} \boldsymbol{b}_{1,lpha}, \dots, \mathbf{V} \boldsymbol{b}_{i-1,lpha}] = \mathbf{U} \mathbf{R} [\boldsymbol{b}_{1,lpha}, \dots, \boldsymbol{b}_{i-1,lpha}].$$

Namely, for all j,

$$\hat{w}_{j,\alpha} = \boldsymbol{b}_{j,\alpha}^{\top} \mathbf{V}^{\top} \mathbf{W}^{-1/2} \boldsymbol{\psi}, \tag{22}$$

with

$$\boldsymbol{b}_{j,\alpha} = \underset{\boldsymbol{b} \in \mathbb{R}^{r \times 1}: \boldsymbol{b}^{\top} \boldsymbol{b} = 1}{\arg \max} (\boldsymbol{b}^{\top} \mathbf{G}_{j}^{\top} \boldsymbol{Y}_{c})^{2} (\boldsymbol{b}^{\top} \mathbf{G}_{j}^{\top} \mathbf{G}_{j} \boldsymbol{b})^{\alpha/(1-\alpha)-1}$$
(23)

$$= \left\{ \mathbf{Y}_{c}^{\top} \mathbf{G}_{j} (\mathbf{G}_{j}^{\top} \mathbf{G}_{j} + \delta_{j,\alpha}^{-1} \zeta_{j,\alpha} \mathbf{I}_{r})^{-2} \mathbf{G}_{j}^{\top} \mathbf{Y}_{c} \right\}^{-1/2} (\mathbf{G}_{j}^{\top} \mathbf{G}_{j} + \delta_{j,\alpha}^{-1} \zeta_{j,\alpha} \mathbf{I}_{r})^{-1} \mathbf{G}_{j}^{\top} \mathbf{Y}_{c}$$

$$(24)$$

in which  $\zeta_{j,\alpha}$  is the largest eigenvalue of  $\mathbf{G}_j^{\top}\mathbf{G}_j$ . The ridge-type (24) is deduced from Björkström and Sundberg (1999, Proposition 2.1). The only unknown  $\delta_{j,\alpha}$  in (24) is the local maximizer in  $(-1,\infty)\setminus\{0\}$  of the univariate function

$$Q_{j,\alpha}(\delta) = \left\{ \mathbf{Y}_{c}^{\top} \mathbf{G}_{j} (\mathbf{G}_{j}^{\top} \mathbf{G}_{j} + \delta^{-1} \zeta_{j,\alpha} \mathbf{I}_{r})^{-1} \mathbf{G}_{j}^{\top} \mathbf{Y}_{c} \right\}^{2}$$

$$\times \left\{ \mathbf{Y}_{c}^{\top} \mathbf{G}_{j} (\mathbf{G}_{j}^{\top} \mathbf{G}_{j} + \delta^{-1} \zeta_{j,\alpha} \mathbf{I}_{r})^{-2} \mathbf{G}_{j}^{\top} \mathbf{Y}_{c} \right\}^{\alpha/(\alpha - 1)}$$

$$\times \left\{ \mathbf{Y}_{c}^{\top} \mathbf{G}_{j} (\mathbf{G}_{j}^{\top} \mathbf{G}_{j} + \delta^{-1} \zeta_{j,\alpha} \mathbf{I}_{r})^{-1} \mathbf{G}_{j}^{\top} \mathbf{G}_{j} \right\}$$

$$(\mathbf{G}_{j}^{\top} \mathbf{G}_{j} + \delta^{-1} \zeta_{j,\alpha} \mathbf{I}_{r})^{-1} \mathbf{G}_{j}^{\top} \mathbf{Y}_{c} \right\}^{\alpha/(1 - \alpha) - 1}$$

and expected to be figured out through an arbitrary computer algebra system, where  $Q_{j,\alpha}(\delta)$  is obtained by plugging (24) back into the maximization objective in (23). Fixing p, we then proceed to an estimator for  $\beta_{p,\alpha}$  (10):

$$\hat{\beta}_{p,\alpha} = [\hat{w}_{1,\alpha}, \dots, \hat{w}_{p,\alpha}] (\mathbf{H}_p^{\top} \mathbf{H}_p)^{-1} \mathbf{H}_p^{\top} \mathbf{Y}_c$$

$$= \boldsymbol{\psi}^{\top} \mathbf{W}^{-1/2} \mathbf{V} [\boldsymbol{b}_{1,\alpha}, \dots, \boldsymbol{b}_{p,\alpha}] (\mathbf{H}_p^{\top} \mathbf{H}_p)^{-1} \mathbf{H}_p^{\top} \mathbf{Y}_c.$$

**Remark 1** Despite the possible ambiguity in representing  $b_{j,\alpha}$  (24), the consistence of  $\hat{w}_{j,\alpha}$  (22) is not affected, as long as (C5) in the appendix is fulfilled; refer to Zhou (2019, Remark 1).

Analogous to  $X_i$ 's, the trajectory to be assigned,  $X^*$ , is discretely observed and has to be estimated by

$$\hat{X}^* = \hat{\boldsymbol{c}}^{*\top} \boldsymbol{\psi},$$

where  $\hat{c}^*$  is available by applying the B-spline smoothing to  $X^*(t_1), \ldots, X^*(t_M)$ . Let  $N_0$  (resp.  $N_1$ ) denote the number of training trajectories belonging to  $\Pi_0$  (resp.  $\Pi_1$ ). Estimating mean functions  $\mu_{[k]}$  by

$$\hat{\mu}_{[k]} = \frac{1}{N_k} \sum_{i=1}^{N} \hat{X}_i \mathbb{1}(X_i \in \Pi_k) = \frac{1}{N_k} \sum_{i=1}^{N} \hat{c}_i^{\top} \psi \mathbb{1}(X_i \in \Pi_k), \tag{25}$$

the empirical CCC-Q and -L are then given by, respectively,

$$\hat{\mathcal{D}}_{Q}(\hat{X}^{*} \mid \hat{\beta}_{p,\alpha}) = \hat{\sigma}_{[1]}^{-2}(\hat{\beta}_{p,\alpha}) \left\{ \int_{\mathcal{T}} \hat{\beta}_{p,\alpha}(\hat{X}^{*} - \hat{\mu}_{[1]}) \right\}^{2}$$

$$- \hat{\sigma}_{[0]}^{-2}(\hat{\beta}_{p,\alpha}) \left\{ \int_{\mathcal{T}} \hat{\beta}_{p,\alpha}(\hat{X}^{*} - \hat{\mu}_{[0]}) \right\}^{2} + 2 \ln \frac{N_{0}\hat{\sigma}_{[1]}(\hat{\beta}_{p,\alpha})}{N_{1}\hat{\sigma}_{[0]}(\hat{\beta}_{p,\alpha})}$$
(26)

and

$$\hat{\mathcal{D}}_{L}(\hat{X}^{*} \mid \hat{\beta}_{p,\alpha}) = \hat{\sigma}_{\text{pool}}^{-2}(\hat{\beta}_{p,\alpha}) \left\{ \int_{\mathcal{T}} \hat{\beta}_{p,\alpha}(\hat{X}^{*} - \hat{\mu}_{[1]}) \right\}^{2} - \hat{\sigma}_{\text{pool}}^{-2}(\hat{\beta}_{p,\alpha}) \left\{ \int_{\mathcal{T}} \hat{\beta}_{p,\alpha}(\hat{X}^{*} - \hat{\mu}_{[0]}) \right\}^{2} + 2 \ln \frac{N_{0}}{N_{1}},$$
 (27)

where, for k = 0, 1,

$$\hat{\sigma}_{\text{pool}}^{2}(\omega) = (N-2)^{-1} \sum_{k=0}^{1} \sum_{i=1}^{N} \left\{ \int_{\mathcal{T}} \omega(\hat{X}_{i} - \hat{\mu}_{[k]}) \right\}^{2} \mathbb{1}(X_{i} \in \Pi_{k}), \quad (28)$$

$$\hat{\sigma}_{[k]}^2(\omega) = (N_k - 1)^{-1} \sum_{i=1}^N \left\{ \int_{\mathcal{T}} \omega(\hat{X}_i - \hat{\mu}_{[k]}) \right\}^2 \mathbb{1}(X_i \in \Pi_k). \tag{29}$$

**Proposition 4** Fix  $p \in \mathbb{Z}^+$  and  $\alpha \in [0,1)$  and assume (C2)–(C5). Empirical classifier  $\hat{\mathcal{D}}_Q(\hat{X}^* \mid \hat{\beta}_{p,\alpha})$  (26) (resp.  $\hat{\mathcal{D}}_L(\hat{X}^* \mid \hat{\beta}_{p,\alpha})$  (27)) converges to its population version  $\mathcal{D}_Q(X^* \mid \beta_{p,\alpha})$  (11) (resp.  $\mathcal{D}_L(X^* \mid \beta_{p,\alpha})$  (13)) in probability as N diverges. Further, if (C1) holds too, a direct corollary is then

$$\lim_{p \to \infty} \lim_{N \to \infty} \operatorname{err} \{ \hat{\mathcal{D}}_L(\hat{X}^* \mid \hat{\beta}_{p,\alpha}) \} = 0.$$

## 2.3.2. Tuning parameter selection

As explained in Section 2.2, this functional classification problem is convertible to a functional linear regression problem when estimating the projection direction. Alternative to the cross-validation, GCV is frequently used in choosing tuning parameters in functional linear models (e.g., Cardot et al., 2003, 2007; Reiss and Ogden, 2010). This GCV-based method is considerably more efficient than cross-validation in computation. In this paper, we suggest searching for the optimal pair of  $(p, \alpha)$  by respectively minimizing

$$GCV(p, \alpha) = \frac{\sum_{i=1}^{N} \left[ Y_i - \mathbb{1} \{ \hat{\mathcal{D}}_Q(\hat{X}_i \mid \hat{\beta}_{p,\alpha}) < 0 \} \right]^2}{(N - p - 2)^2}$$

and

$$GCV(p,\alpha) = \frac{\sum_{i=1}^{N} \left[ Y_i - \mathbb{1} \{ \hat{\mathcal{D}}_L(\hat{X}_i \mid \hat{\beta}_{p,\alpha}) < 0 \} \right]^2}{(N - p - 2)^2}$$

for CCC-Q and -L with respect to  $(p, \alpha)$ , where the digit 2 in parenthesis in the denominator corresponds to the number of populations. Algorithm 1 details the implementation of CCC with the proposed GCV-based tuning scheme.

Rather than the usual rectanglar search grid, the candidate pool for  $(p,\alpha)$  here, say  $\{(p,\alpha):p\in\{1,\ldots,p_{\max,\alpha}\},\alpha\in\{\alpha_1,\ldots,\alpha_J\}\subset[0,1)\}$ , is nonrectanglar and set up in a random way: for each  $\alpha\in\{\alpha_1,\ldots,\alpha_J\}$  (=  $\{0\times10^{-1},\ldots,9\times10^{-1},1-10^{-2},\ldots,1-10^{-4}\}$  in Section 3),  $p_{\max,\alpha}$  is randomly picked up from Unif $\{1,\ldots,p_{\mathrm{upper}}\}$ , where  $p_{\mathrm{upper}}$  can be determined by

$$p_{\text{upper}} = \min \left\{ j_0 \in \mathbb{Z}^+ : \sum_{j=1}^{j_0} \hat{\lambda}_j^W / \sum_{j=1}^{\infty} \hat{\lambda}_j^W \ge 99\% \right\}$$
 (30)

in which  $\hat{\lambda}_{j}^{W}$  estimates the jth top eigenvalue of  $v_{X}^{W}$  at (4). The random grid is typically of smaller cardinality and hence leads to less running time. Zhou (2019, Section 5) illustrated that this strategy was accompanied with little loss in prediction accuracy.

#### 3. NUMERICAL ILLUSTRATION

In spite of theoretical arguments illustrating the asymptotically perfect classification of CCC-L in specific cases, we were still in need of more evidences to support our proposals, especially CCC-Q. We then resorted to numerical studies in order to compare the performance of PCC, PLCC and two CCC classifiers in finite-sample applications. Numbers of FPC (resp. FPLS) basis functions for PCC (resp. PLCC) was selected from  $\{1, \ldots, p_{\text{upper}}\}$  through 5-fold

cross-validation. Two more classifiers (viz. functional versions of logit regression and naive bayes) were involved too in the comparison and both implemented through R-package fda.usc (Febrero-Bande and Oviedo de la Fuente, 2012). Our code trunks are publicly available at https://github.com/ZhiyangGeeZhou/CCC.

## 3.1. Simulation study

We generated R=200 samples, each containing N=200 curves  $X_i$ ,  $i=1,\ldots,200$ . In each sample, we randomly preserved 80% curves for training and left for testing. Each curve was spotted at 101 equally spaced points in  $\mathcal{T}=[0,1]$ , i.e.,  $\{0,1/100,\ldots,99/100,1\}$ , and iid as

$$X_i = \sum_{k=0}^{1} \left( \sum_{j=1}^{5} \lambda_{k,j}^{1/2} Z_{ij} \phi_{k,j} + \mu_{[k]} \right) \mathbb{1}(X_i \in \Pi_k).$$

Without loss of generality, the difference of two mean functions was set to be exactly  $\mu_{[1]}$ , i.e.,  $\mu_{[0]}(\cdot) \equiv 0$ . Instead of a mixture of Gaussian processes, a setup without normality was considered:  $Z_{ij} \sim \exp(1) - 1$ ,  $i = 1, \ldots, N$ ,  $j = 1, \ldots, 5$ . Although sub-covariance functions  $v_X^{[0]}$  and  $v_X^{[1]}$  shared the identical nonzero eigenvalues 200, 100, 1, .2, .1, they might differ in eigenfunctions; specifically, we took the (normed-to-one) jth-order shifted Legendre polynomial (see, e.g., Hochstrasser, 1972, pp. 773–774) as the jth eigenfunction of  $v_X^{[0]}$ , i.e.,

$$\phi_{0,1}(t) = \sqrt{3}(2t - 1),$$

$$\phi_{0,2}(t) = \sqrt{5}(6t^2 - 6t + 1),$$

$$\phi_{0,3}(t) = \sqrt{7}(20t^3 - 30t^2 + 12t - 1),$$

$$\phi_{0,4}(t) = 3(70t^4 - 140t^3 + 90t^2 - 20t + 1),$$

$$\phi_{0,5}(t) = \sqrt{11}(252t^5 - 630t^4 + 560t^3 - 210t^2 + 30t - 1).$$

As a result,  $p_{\rm upper}$ , the upper bound of number of components, was set to 5 directly (rather than following (30)). We meanwhile accounted for two sorts of combinations of  $\mu_{[1]}$  and  $\phi_{1,j}$ :

(i) 
$$\mu_{[1]} = \rho \lambda_{1,1}^{1/2} \phi_{1,1}$$
 and  $\phi_{0,j} = \phi_{1,j}$ ,

(ii) 
$$\mu_{[1]} = \rho \lambda_{1,3}^{1/2} \phi_{1,3}$$
 and  $\phi_{0,5-j} = \phi_{1,j}$ .

In both scenarios,  $\rho$  (= 1, 10) controlled the magnitude of gap  $\mu_{[1]} - \mu_{[0]}$  as well as the ratio of between-group variation to within-group one. Despite the common adoption of  $\pi_0 = \Pr(X_i \in \Pi_0) = 50\%$  in literature, we checked as well unbalanced arrangement like  $\pi_0 = 80\%$ . These in total eight setting combinations would help us clarify the joint impact from  $\rho$ ,  $\pi_0$  and  $\mu_{[1]} - \mu_{[0]}$  on misclassification.

Regardless of values of  $\rho$  and  $\pi_0$ , design (i) equally favored all the classifiers here (see Figure 2), as  $\mu_{[1]} - \mu_{[0]}$  was parallel to the top eigenfunction of not only  $v_X$  at (3) but also  $v_X^W$  at (4). The value of  $\rho$  matters a lot for design (i): in Figure 1a (with  $\rho=1$ ), the two sub-populations merged together, accompanying with extremely high misclassification rate which may even worse than a random guess in the case of  $\pi_0=80\%$  (see the second row of Table 1);  $\rho=10$  made the

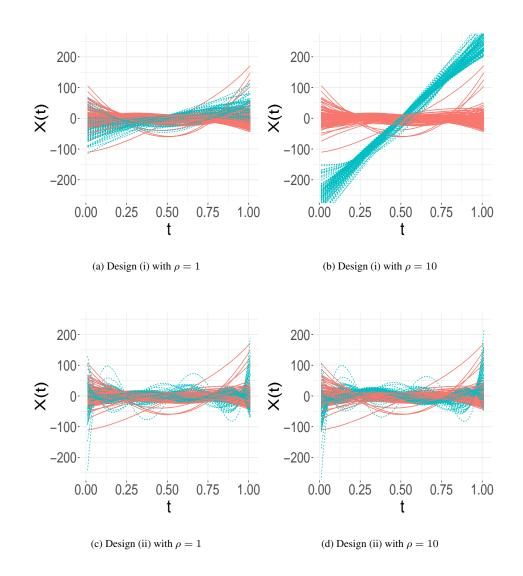
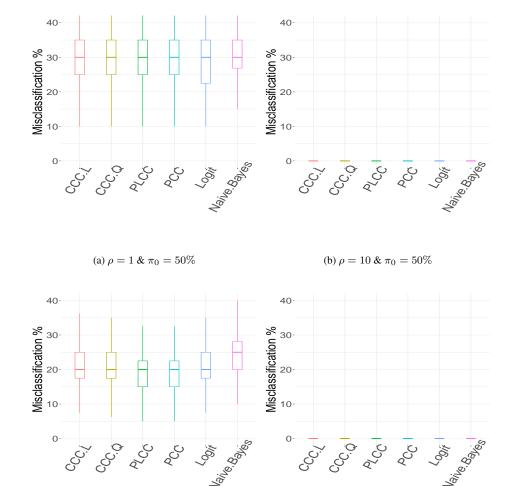


FIGURE 1: : Samples following the simulation designs. Each subfigure displays a sample with red solid trajectories from  $\Pi_0$  and blue dashed ones from  $\Pi_1$ .

two sub-populations visibly separable and hence corresponded to error rates of a fairly low level (see Figures 2b and 2d).

It was a different story for design (ii). It restricted  $\mu_{[1]} - \mu_{[0]}$  to be parallel to  $\phi_{0,3}$  which is the least important eigenfunction of



(c)  $\rho = 1 \& \pi_0 = 80\%$  (d)  $\rho = 10 \& \pi_0 = 80\%$ 

FIGURE 2: : Boxplots of misclassification percentage for design (i). In each panel, the six boxes, from left to right, correspond to classifiers CCC-L, CCC-Q, PLCC, PCC, (functional) logit regression and (functional) naive bayes, respectively. The four subfigures come with the identical scale.

$$v_X^W(s,t) = 160.02\phi_{0,1}(s)\phi_{0,1}(t) + 80.04\phi_{0,2}(s)\phi_{0,2}(t)$$
$$+ 40.08\phi_{0,5}(s)\phi_{0,5}(t) + 20.16\phi_{0,4}(s)\phi_{0,4}(t) + \phi_{0,3}(s)\phi_{0,3}(t).$$

In this case, focused only on decomposing  $v_X^W$  at (4), PCC probably failed to extract the correct direction of  $\mu_{[1]} - \mu_{[0]}$  and naturally yielded more misclassification regardless of  $\rho$  or  $\pi_0$ . Moreover,  $v_X^{[1]}$  shared the same eigenfunctions with  $v_X^{[0]}$  but in a reversed order, violating the assumption of CCC-L and PLCC. Due to the magnitude of  $\lambda_{1,3}$ , the two subgroups appeared not separable even for  $\rho=10$  (see Figure 1). Actually, trajectories from sub-population  $\Pi_1$  were more bumpy; this feature would become more obvious for larger  $\rho$ , e.g,  $\rho=100$  (not illustrated here). When  $\rho=1$ , CCC-Q significantly outperformed the other competitors here; see Figures 3a and 3c. As  $\rho$  grew up to 10, the performance of classifiers was generally improved, though PLCC and PCC still output pretty high misclassification rate (see the last two rows of Table 2 and Figures 3b and 3d). If we further enlarged  $\rho$  to, e.g., 100, the identification became no longer challenging even for PLCC and PCC.

### 3.2. Real data application

For each dataset, we repeated a random split with ratio 8:2 for 200 times: each time we trained classifiers with 80% data points and then tested them on the remaining 20%. Table 2 summarized the means and standard deviations of misclassification percentages.

The first real example treated  $Tecator^{TM}$  data (accessible at http://lib.stat.cmu.edu/datasets/tecator on February 12, 2021). This dataset was collected by  $Tecator^{TM}$  Infratec Food and Feed Analyzer (and hence named).

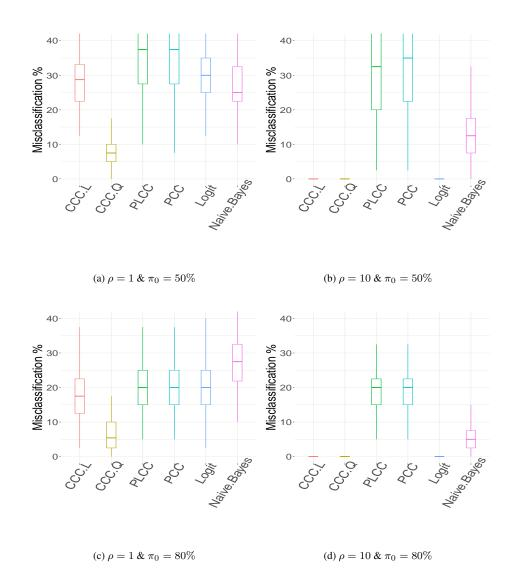


FIGURE 3: : Boxplots of misclassification percentage for design (ii). In each panel, the six boxes, from left to right, correspond to classifiers CCC-L, CCC-Q, PLCC, PCC, (functional) logit regression, and (functional) naive bayes, respectively. The four subfigures come with the identical scale.

It consisted of near infrared absorbance spectra (i.e., the logarithm to base 10 of transmittance at each wavelength) of 240 fine-chopped pure meat samples. Each spectrum ranged from 850 to 1050 nm and was spotted at 100 "time points" (viz.

TABLE 1: Mean misclassification percentage (%) (with standard deviations in parentheses) for various settings and classifiers. The last six columns, from left to right, correspond to classifiers CCC-L, CCC-Q, PLCC, PCC, (functional) logit regression and (functional) naive bayes, respectively.

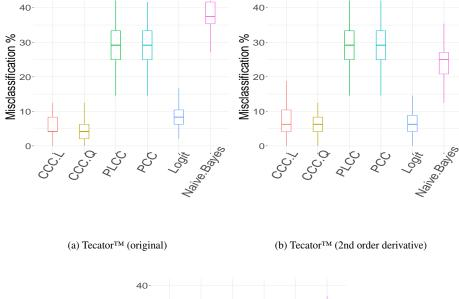
Design	ρ	$\pi_0$	CCC-L	CCC-Q	PLCC	PCC	Logit	Naive Bayes
(i)	1	50%	30 (8.2)	30 (8.6)	31 (7.1)	31 (7.3)	30 (8.0)	31 (7.9)
(i)	1	80%	21 (5.9)	21 (6.0)	20 (5.9)	20 (6.0)	21 (5.9)	24 (6.6)
(i)	10	50%	.13 (.56)	.15 (.60)	.19 (1.0)	.11 (.52)	.09 (.46)	.15 (.60)
(i)	10	80%	.22 (.70)	.22 (.72)	.31 (1.1)	.25 (.75)	.11 (.52)	.24 (.78)
(ii)	1	50%	29 (7.8)	7.4 (4.1)	38 (14)	37 (14)	29 (8.0)	27 (7.9)
(ii)	1	80%	17 (7.0)	6.7 (4.0)	20 (6.1)	20 (6.2)	20 (6.8)	27 (8.3)
(ii)	10	50%	.22 (.73)	.21 (.62)	33 (15)	35 (15)	.11 (.52)	13 (6.9)
(ii)	10	80%	.23 (.70)	.25 (.79)	20 (6.3)	20 (6.7)	.14 (.57)	5.3 (4.4)

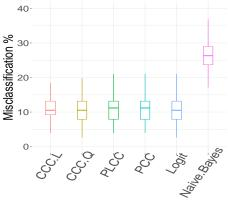
channels). Additionally, three contents, water, protein and fat, were recorded in percentage for each piece of meat. In our study, meat samples were categorized into two groups:  $\Pi_1$  was comprised of meat samples with protein content less than 16% and the rest constituted  $\Pi_0$ . The 240 spectrum curves (or their second order derivative curves as recommended by Ferraty and Vieu, 2006, Section 7.2.2) were regarded as functional covariates in the study. For both sorts of trajectories, the classification output was analogous to that for simulated design (ii) with  $\rho=10$ : CCC subtypes and (functional) logit regression yielded considerably less errors than the other three classifiers; compare Figures 3b, 3d, 4a and 4b.

TABLE 2: : Average misclassification percentage for real datasets (with standard deviations in parentheses) corresponding to different classifiers. The last six columns correspond to classifiers CCC-L, CCC-Q, PLCC, PCC, (functional) logit regression, and (functional) naive bayes, respectively. Ties at the last row are caused by rounding.

	CCC-L	CCC-Q	PLCC	PCC	Logit	Naive Bayes
Tecator <sup>TM</sup> (original)	5.5 (3.3)	4.6 (2.8)	30 (6.5)	29 (6.8)	8.8 (4.0)	39 (6.6)
Tecator <sup>TM</sup> (2nd order derivative)	7.3 (4.4)	6.0 (3.4)	30 (6.5)	30 (6.5)	7.0 (3.6)	24 (5.9)
DTI	11 (3.5)	11 (3.5)	11 (3.6)	11 (3.6)	11 (3.7)	26 (4.5)

We returned to DTI mentioned in Section 1. Measured through DTI, the fractional anisotropy, a scalar ranging from 0 to 1, is used to reflect the fiber density, axonal diameter and myelination in white matter. Along a tract of interest, fractional anisotropy values form a curve, viz. a tract fractional anisotropy profile. We analyzed dataset DTI in R-package refund (Goldsmith et al., 2019). It was initially collected at Johns Hopkins University and the Kennedy-Krieger Institute, containing tract fractional anisotropy profiles (measured at 93 locations) for corpus callosum of healthy people ( $\Pi_0$ ) and MS patients ( $\Pi_1$ ) and involving 382 subjects in total. By classifying these profiles (with missing values imputed through local polynomial regression), we tried to identify the status of each subject: healthy or suffering from MS. Except for the (functional) naive bayes, classifiers reached a tie after rounding (see the last row of Table 2), i.e., they enjoyed fairly close classification accuracy in identifying MS patients.





(c) DTI

FIGURE 4: : Boxplots of misclassification percentages for Tecator<sup>™</sup> and DTI data. The top two panels reflect respective results with original and second order derivative curves. In each panel, the four boxes, from left to right, correspond to classifiers CCC-L, CCC-Q, PLCC, PCC, (functional) logit regression, and (functional) naive bayes, respectively. The three subfigures are displayed with the identical scale.

# 4. CONCLUSION AND DISCUSSION

We propose two subtypes of CCC classifiers, viz. CCC-L and -Q, for binary classification of curves. Theoretically, under certain circumstances, CCC-L enjoys

the (asymptotic) zero misclassification regardless of the distribution assumption, while, in certain empirical studies, CCC-Q seems superior to CCC-L and other competitors. Once regularity conditions are met, our proposal results in empirical classifiers which are consistent to their theoretical counterparts, for the case of "fixed p and infinite N".

In the numerical experiments in Section 3, we do see benefits from the introduction of the supervision controller  $\alpha$ . Nevertheless, one cannot be too optimistic; actually, tuning one more parameter may yield more variation and even bias. In addition, the projection direction  $\beta_{p,\alpha}$  at (10) potentially becomes unstable for large p, since  $w_{p,\alpha}$  is constructed iteratively without penalty. Nevertheless, the introduction of one more hyperparameter would force our implementation to be more computationally involved.

One may be concerned about the chosen values of hyperparameters for our proposed classifiers. In most cases of numerical study, hyperparameter  $\alpha$  (resp. p) for CCC-L and -Q ended with similar values; exceptions arose for design (ii) with  $\rho=1$  (where CCC-Q outperformed CCC-L significantly). Specifically, in that case, CCC-Q picked up mean  $\alpha$  around .7, whereas CCC-L chose about .5 and hence yielded a classification accuracy comparable with PLCC. As for the size of basis, CCC subtypes seemed even more "parsimonious" than PLCC, mostly utilizing less than 3 basis functions.

Regarding a further extension to the functional classification with  $K \geq 3$  classes, one naive strategy is to carry out binary classifiers repeatedly. To be explicit, for a newcomer  $X^*$ , each time we only consider two distinct labels and then assign either label to it, or equivalently, throw a vote for either of the two labels. After all  $\binom{K}{2}$  binary classifications, the label that wins the most votes is eventually assigned to  $X^*$ . Another route is embedding FC basis into the iteratively reweighted least squares (Green, 1984). In that way, the resulting modification could be utilized for estimating generalized linear models with functional covariates.

# **BIBLIOGRAPHY**

Björkström, A. and Sundberg, R. (1999). A generalized view on continuum regression. *Scandinavian Journal of Statistics*, 26, 17–30.

Cardot, H., Crambes, C., Kneip, A., and Sarda, P. (2007). Smoothing splines estimators in functional linear regression with errors-in-variables. *Computational Statistics & Data Analysis*, 51, 4832–4848.

Cardot, H., Ferraty, F., and Sarda, P. (2003). Spline estimators for the functional linear model. *Statistica Sinica*, 13, 571–591.

Chui, C. K. (1971). Concerning rates of convergence of Riemann sums. *Journal of Approximation Theory*, 4, 279–287.

Craven, P. and Wahba, G. (1979). Smoothing noisy data with spline functions. *Numerische Mathematik*, 31, 377–403.

Dai, X., Müller, H.-G., and Yao, F. (2017). Optimal Bayes classifiers for functional data and density ratios. *Biometrika*, 104, 3, 545–560.

de Boor, C. (2001). A Practical Guide to Splines. Applied Mathematical Sciences. Springer, New York, revised ed.

Delaigle, A. and Hall, P. (2012). Achieving near perfect classification for functional data. *Journal of the Royal Statistical Society Series B*, 74, 267–286.

Fan, J., Feng, Y., and Tong, X. (2012). A road to classification in high dimensional space: the regularized optimal affine discriminant. *Journal of the Royal Statistical Society Series B*, 74, 745–771.

Febrero-Bande, M. and Oviedo de la Fuente, M. (2012). Statistical computing in functional data analysis: The R package fda.usc. *Journal of Statistical Software*, 51, 4, 1–28.

Ferraty, F. and Vieu, P. (2003). Curves discrimination: a nonparametric functional approach. *Computational Statistics & Data Analysis*, 44, 161–173.

— (2006). *Nonparametric Functional Data Analysis: Theory and Practice*. Springer Series in Statistics. Springer, New York.

Galeano, P., Joseph, E., and Lillo, R. E. (2015). The Mahalanobis distance for functional data with applications to classification. *Technometrics*, 57, 281–291.

Goldsmith, J., Crainiceanu, C. M., Caffo, B., and Reich, D. (2012). Longitudinal penalized functional regression for cognitive outcomes on neuronal tract measurements. *Journal of the Royal Statistical Society Series C*, 61, 453–469.

Goldsmith, J., Scheipl, F., Huang, L., Wrobel, J., Di, C., Gellar, J., Harezlak, J., McLean, M. W., Swihart, B., Xiao, L., Crainiceanu, C., and Reiss, P. T. (2019). *refund: Regression with Functional Data*. R package version 0.1-21.

Green, P. J. (1984). Iteratively reweighted least squares for maximum likelihood estimation, and some robust and resistant alternatives. *Journal of the Royal Statistical Society Series B*, 46, 149–192.

Hochstrasser, W. (1972). Orthogonal polynomials. In M. Abramowitz and I. A. Stegun (Eds.) Handbook of Mathematical Functions: With Formulas, Graphs, and Mathematical Tables, National Bureau of Standards, Washington D.C., 771–802. 10th printing.

Jung, S. (2018). Continuum directions for supervised dimension reduction. *Computational Statistics & Data Analysis*, 125, 27–43.

Leng, X. and Müller, H.-G. (2005). Classification using functional data analysis for temporal gene expression data. *Bioinformatics*, 22, 68–76.

Lyche, T., Manni, C., and Speleers, H. (2018). Foundations of spline theory: B-splines, spline approximation, and hierarchical refinement. In A. Kunoth, T. Lyche, G. Sangalli, and S. Serra-Capizzano (Eds.) *Splines and PDEs: From Approximation Theory to Numerical Linear Algebra*, Springer, Cham, Switzerland, 1–76.

Ramsay, J. O. and Silverman, B. W. (2005). *Functional Data Analysis*. Springer, New York, 2nd ed.

Reiss, P. T. and Ogden, R. T. (2010). Functional generalized linear models with images as predictors. *Biometrics*, 66, 61–69.

Rossi, F. and Villa, N. (2006). Support vector machine for functional data classification. *Neurocomputing*, 69, 730–742.

Sbardella, E., Tona, F., Petsas, N., and Pantano, P. (2013). DTI measurements in Multiple Sclerosis: evaluation of brain damage and clinical implications. *Multiple Sclerosis International*, 2013. Article ID 671730.

Shin, H. (2008). An extension of Fisher's discriminant analysis for stochastic processes. *Journal of Multivariate Analysis*, 99, 1191–1216.

Utreras, F. (1983). Natural spline functions, their associated eigenvalue problem. *Numerische Mathematik*, 42, 107–117.

Zhou, Z. (2019). Functional continuum regression. *Journal of Multivariate Analysis*, 173, 328–346.

# **APPENDIX**

Our theoretical perspectives are built upon the following assumptions.

(C1) 
$$\{\int_{\mathcal{T}} \beta_{p,\alpha}(\mu_{[1]} - \mu_{[0]})\}^2 / \operatorname{var}\{\int_{\mathcal{T}} \beta_{p,\alpha}(X - \mu_{[k]}) \mid X \in \Pi_k\}$$
 diverges as  $p \to \infty$  for each  $\alpha$  and  $k$ .

- (C2) Realizations of X is twice continuously differentiable and ||X'|| is bounded almost surely.
- (C3)  $\tau_1, \ldots, \tau_L$  are eigenvalue of  $\mathbf{Pen}^{-1/2}\mathbf{WPen}^{-1/2}$  such that  $\tau_1 = \tau_2 = 0$ ,  $\tau_3 \geq \cdots \geq \tau_L$ , and  $C_1(l-2)^{-4} \leq \tau_l \leq C_2(l-2)^{-4}$  for  $l \geq 3$ , with neither  $C_1$  nor  $C_2$  depending on l or L.

(C4)  $M \to \infty$  and  $M^{-1}\theta_0 \to 0$  as  $N \to \infty$ , where  $\theta_0 > 0$  is the smoothing parameter for all trajectories.

(C5) For all  $j \in \operatorname{rank}(\hat{\mathbf{C}}_{c}\mathbf{W}^{1/2})$ ,  $T_{j,\alpha}(w)$  attains a unique maximizer (up to sign) in  $\{w \in L^{2}(\mathcal{T}) : ||w|| = 1\}$ .

Condition (C1) implies that, after projected to the direction of  $\beta_{p,\alpha}$ , as p diverges, the within-group covariance becomes more and more ignorable when compared with the between-group one, i.e., the two groups become more and more separable. It is analogous to assumption (4.4)(d) of Delaigle and Hall (2012) and assures us of the (asymptotic) perfect classification of CCC-L. Assumptions (C2) and (C3) jointly guarantee that the smoothed curves converge to the true ones as observations become denser and denser; although the latter one has been proved by Utreras (1983, eq. 4) for natural splines, we have little knowledge on whether it still holds for B-splines and hence have to assume it following Craven and Wahba (1979, eq. A4.3.1). If we have extra regularity conditions (C4) and (C5), the proposed empirical implementation in Section 2.3.1 turns out to be consistent in probability.

Proof of Proposition 1. Write  $\gamma_{p,\alpha}=\int_{\mathcal{T}}\beta_{p,\alpha}(\mu_{[1]}-\mu_{[0]})$  and  $R_{p,\alpha}^{[k]}=\int_{\mathcal{T}}\beta_{p,\alpha}(X^*-\mu_{[k]})$ . Recalling (12),  $\sigma_{[k]}^2(\beta_{p,\alpha})=\mathrm{var}(R_{p,\alpha}^{[k]}\mid X\in\Pi_k),\ k=0,1.$  Thus,

$$\Pr\{\mathcal{D}_L(X^* \mid \beta_{p,\alpha}) < 0 \mid X^* \in \Pi_0\}$$

$$= \Pr\left\{ (R_{p,\alpha}^{[0]} - \gamma_{p,\alpha})^2 - (R_{p,\alpha}^{[0]})^2 < 2\sigma_{[0]}^2(\beta_{p,\alpha}) \ln \frac{1 - \pi_0}{\pi_0} \, \middle| \, X^* \in \Pi_0 \right\}$$

$$= \Pr\left[ \frac{R_{p,\alpha}^{[0]}}{\sigma_{[0]}(\beta_{p,\alpha})} > \frac{\gamma_{p,\alpha}^2 + 2\sigma_{[0]}^2(\beta_{p,\alpha}) \ln \{\pi_0/(1 - \pi_0)\}}{2\gamma\sigma_{[0]}(\beta_{p,\alpha})} \, \middle| \, X^* \in \Pi_0 \right]$$

$$\leq \frac{4\sigma_{[0]}^2(\beta_{p,\alpha})/\gamma_{p,\alpha}^2}{\left[1 + 2\gamma_{p,\alpha}^{-2}\sigma_{[0]}^2(\beta_{p,\alpha}) \ln \{\pi_0/(1 - \pi_0)\}\right]^2},$$

where the upper bound is derived from Chebyshev's inequality and the identity that  $R_{p,\alpha}^{[0]}/\sigma_{[0]}(\beta_{p,\alpha})$  (conditional on the event  $X^* \in \Pi_0$ ) is of zero mean and unit variance. Similarly, we deduce that

$$\Pr\{\mathcal{D}_L(X^* \mid \beta_{p,\alpha}) > 0 \mid X^* \in \Pi_1\} \le \frac{4\sigma_{[1]}^2(\beta_{p,\alpha})/\gamma_{p,\alpha}^2}{\left[1 + 2\gamma_{p,\alpha}^{-2}\sigma_{[0]}^2(\beta_{p,\alpha})\ln\{(1 - \pi_0)/\pi_0\}\right]^2}.$$

Eventually, as p diverges, the zero-convergence of

$$\operatorname{err}\{\mathcal{D}_{L}(X^{*} \mid \beta_{p,\alpha})\} = \pi_{0} \operatorname{Pr}\{\mathcal{D}_{L}(X^{*} \mid \beta_{p,\alpha}) < 0 \mid X^{*} \in \Pi_{0}\}$$
$$+ (1 - \pi_{0}) \operatorname{Pr}\{\mathcal{D}_{L}(X^{*} \mid \beta_{p,\alpha}) > 0 \mid X^{*} \in \Pi_{1}\}$$

results from (C1) (i.e.,  $\sigma^2_{[k]}(\beta_{p,\alpha})/\gamma^2_{p,\alpha} \to 0$  as p diverges for each  $\alpha$  and k).

Proof of Proposition 2. Recall  $\Delta t = (t_{\text{max}} - t_{\text{min}})/M$  and matrices  $\psi$  (16),  $\hat{c}_i$  (17),  $\Psi$  (18), W (20) and Pen (19), all defined in Section 2.3.1. Introduce operator  $\mathcal{P}_{BS_L}$  such that, for each  $f \in L^2(\mathcal{T})$ ,  $\mathcal{P}_{BS_L}f$  is the orthogonal projection of f onto  $BS_L$  of (14), i.e.,

$$\mathcal{P}_{BS_L}f = \left[\int_{\mathcal{T}} f\psi_1, \dots, \int_{\mathcal{T}} f\psi_L 
ight] \mathbf{W}^{-1} oldsymbol{\psi}.$$

For each i, specifically,  $\mathcal{P}_{BS_L} X_i = c_i^{\top} \psi$  with

$$c_i = \mathbf{W}^{-1} \left[ \int_{\mathcal{T}} X_i \psi_1, \dots, \int_{\mathcal{T}} X_i \psi_L \right]^{\top}.$$

We chop  $\|\hat{X}_i - X_i\|$  into two segments:  $\|\mathcal{P}_{BS_L}X_i - X_i\|$  and  $\|\hat{X}_i - \mathcal{P}_{BS_L}X_i\|$ . Combined with Lyche et al. (2018, Theorem 16), condition (C2) implies

$$\|\mathcal{P}_{BS_L}X_i - X_i\| = O_p(\Delta t) = O_p(M^{-1})$$
 as  $M \to \infty$ .

Further, condition (C2) allows us to follow Chui (1971, Theorem 5) to verify that, as  $M \to \infty$ ,  $\|\mathbf{W} - \Delta t \mathbf{\Psi}^{\top} \mathbf{\Psi}\|_F^2 = O(M^{-2})$ ,  $\|\mathbf{W} - \Delta t \mathbf{\Psi}^{\top} \mathbf{\Psi} - \Delta t \theta_0 \mathbf{Pen}\|_F^2 = O(1)$ , and

$$\left\| \left[ \int_{\mathcal{T}} X_i \psi_1, \dots, \int_{\mathcal{T}} X_i \psi_L \right]^{\top} - \Delta t \boldsymbol{X}_i^{\top} \boldsymbol{\Psi} \right\|_{F}^{2} = O_p(M^{-3}),$$

where  $\|\cdot\|_F$  denotes the Frobenius norm. Let  $\tau_1, \ldots, \tau_L$  be eigenvalues of

$$\mathbf{Z} = \mathbf{Pen}^{-1/2}\mathbf{WPen}^{-1/2}$$

with corresponding eigenvectors  $e_1, \ldots, e_L$ . Note the finiteness of both  $\lim_{L\to\infty} \max_{l_1,l_2} |\int_{\mathcal{T}} \psi_{l_1} \psi_{l_2}|$  and  $\lim_{L\to\infty} \max_{l_1,l_2} |\int_{\mathcal{T}} \psi''_{l_1} \psi''_{l_2}|$ . Thus the squared second trunk is

$$\begin{split} &\|\hat{X}_{i} - \mathcal{P}_{BSL}X_{i}\|^{2} \\ &= (\hat{\boldsymbol{c}}_{i}^{\top} - \boldsymbol{c}_{i}^{\top})\mathbf{W}(\hat{\boldsymbol{c}}_{i} - \boldsymbol{c}_{i}) \\ &= \left\{ \Delta t \boldsymbol{X}_{i}^{\top} \boldsymbol{\Psi} (\Delta t \boldsymbol{\Psi}^{\top} \boldsymbol{\Psi} + \Delta t \theta_{0} \mathbf{Pen})^{-1} - \boldsymbol{c}_{i}^{\top} \right\} \mathbf{W} \left\{ (\Delta t \boldsymbol{\Psi}^{\top} \boldsymbol{\Psi} + \Delta t \theta_{0} \mathbf{Pen})^{-1} \Delta t \boldsymbol{\Psi}^{\top} \boldsymbol{X}_{i} - \boldsymbol{c}_{i} \right\} \\ &= \boldsymbol{c}_{i}^{\top} \mathbf{Pen}^{1/2} \left\{ \mathbf{Z} \left( \mathbf{Z} + \Delta t \theta_{0} \mathbf{I}_{L} \right)^{-1} - \mathbf{I}_{L} \right\} \mathbf{Z} \left\{ (\mathbf{Z} + \Delta t \theta_{0} \mathbf{I}_{L})^{-1} \mathbf{Z} - \mathbf{I}_{L} \right\} \mathbf{Pen}^{1/2} \boldsymbol{c}_{i} + o_{p}(1) \end{split}$$

$$= (\Delta t)^{2} \theta_{0}^{2} \boldsymbol{c}_{i}^{\mathsf{T}} \mathbf{Pen}^{1/2} \left( \mathbf{Z} + \Delta t \theta_{0} \mathbf{I}_{L} \right)^{-1} \mathbf{Z} \left( \mathbf{Z} + \Delta t \theta_{0} \mathbf{I}_{L} \right)^{-1} \mathbf{Pen}^{1/2} \boldsymbol{c}_{i} + o_{p}(1)$$

$$= \sum_{l=1}^{L} \frac{\tau_{l}}{(\theta_{0}^{-1} \Delta t^{-1} \tau_{l} + 1)^{2}} (\boldsymbol{c}_{i}^{\mathsf{T}} \mathbf{Pen}^{1/2} \boldsymbol{e}_{l})^{2} + o_{p}(1)$$

$$\leq \Delta t \theta_{0} \sum_{l=1}^{L_{1}-1} \tau_{l} (\boldsymbol{c}_{i}^{\mathsf{T}} \mathbf{Pen}^{1/2} \boldsymbol{e}_{l})^{2} + \sum_{l=L_{1}}^{L} \tau_{l} (\boldsymbol{c}_{i}^{\mathsf{T}} \mathbf{Pen}^{1/2} \boldsymbol{e}_{l})^{2} + o_{p}(1)$$

$$= o_{p}(1) \quad \text{as} \quad M \to \infty,$$

where  $L_1 \in \mathbb{Z}^+$  is so defined that  $\tau_{L_1} = \max\{\tau_L, (\Delta t \theta_0)^{1/2}\}$  and diverges as  $M \to \infty$  owing to (C3).

Proof of Proposition 3. Recall  $\mathcal{P}_{BS_L}$  defined in the proof of Proposition 2. Writing  $\hat{w}_{j,\alpha} = \mathcal{P}_{BS_L}\hat{w}_{j,\alpha} + (\mathcal{I} - \mathcal{P}_{BS_L})\hat{w}_{j,\alpha}$ , with identity operator  $\mathcal{I}$ , one has  $0 < \|\mathcal{P}_{BS_L}\hat{w}_{j,\alpha}\| \le 1$  and  $\int_{\mathcal{T}}\hat{X}_i\mathcal{P}_{BS_L}\hat{w}_{j,\alpha} = \int_{\mathcal{T}}\hat{X}_i\hat{w}_{j,\alpha}$  since  $\hat{X}_i \in BS_L$  for all i. If  $0 < \|\mathcal{P}_{BS_L}\hat{w}_{j,\alpha}\| < 1$  (i.e.,  $(\mathcal{I} - \mathcal{P}_{BS_L})\hat{w}_{j,\alpha} > 0$ ), then  $\mathcal{P}_{BS_L}\hat{w}_{j,\alpha}/\|\mathcal{P}_{BS_L}\hat{w}_{j,\alpha}\|$  satisfies that

$$\hat{T}_{j,\alpha}\left(\frac{\mathcal{P}_{BS_L}\hat{w}_{j,\alpha}}{\|\mathcal{P}_{BS_L}\hat{w}_{j,\alpha}\|}\right) = \|\mathcal{P}_{BS_L}\hat{w}_{j,\alpha}\|^{2\alpha/(\alpha-1)}\hat{T}_{j,\alpha}(\hat{w}_{j,\alpha}) > \hat{T}_{\alpha}(\hat{w}_{j,\alpha}),$$

which violates the definition of  $\hat{w}_{j,\alpha}$  (22). This contradiction implies that  $(\mathcal{I} - \mathcal{P}_{BS_L})\hat{w}_{j,\alpha}$  must be 0.

Proof of Proposition 4. Under conditions (C2)–(C5), fixing p, Proposition 2 and Zhou (2019, Theorem 1) assure us of the zero-convergence (in probability) of  $\|\hat{\beta}_{p,\alpha} - \beta_{p,\alpha}\|$  as N diverges. Since Proposition 2 applies to  $X^*$ , the convergence of empirical classifiers follows.

Received 8 May 2020

Accepted 28 Jan 2021

# Algorithm 1 CCC tuned via GCV

- 1:  $p_{\text{max}} \leftarrow$  upper bound of number of FC basis functions.
- 2: **for**  $\alpha$  in a finite set **do**
- 3: **for** p from 1 to  $p_{\max,\alpha}$  **do**
- 4: **if** p = 1 **then**
- 5:  $\mathbf{P} \leftarrow \mathbf{I}_N$
- 6:  $\mathbf{U}\mathbf{R}\mathbf{V}^{\top} \leftarrow \text{thin singular value decomposition of } \hat{\mathbf{C}}_{c}\mathbf{W}^{1/2}$
- 7:  $\mathbf{G}_1 \leftarrow \mathbf{U}\mathbf{R}$
- 8: **else**

9: 
$$\mathbf{P} \leftarrow \mathbf{P} \{ \mathbf{I}_N - \mathbf{G}_{p-1} \boldsymbol{b}_{p-1,\alpha} (\boldsymbol{b}_{p-1,\alpha}^\top \mathbf{G}_{p-1}^\top \mathbf{G}_{p-1} \boldsymbol{b}_{p-1,\alpha})^{-1} \boldsymbol{b}_{p-1,\alpha}^\top \mathbf{G}_{p-1}^\top \}$$

- 10: end if
- 11:  $\mathbf{G}_n \leftarrow \mathbf{PG}_1$
- 12:  $\zeta \leftarrow \text{largest eigenvalue of } \mathbf{G}_p^{\top} \mathbf{G}_p$

13: 
$$\mathbf{L}(\delta) \leftarrow (\mathbf{G}_n^{\top} \mathbf{G}_p + \delta^{-1} \zeta \mathbf{I}_r)^{-1}$$

14: 
$$Q(\delta) \leftarrow \frac{\{\mathbf{Y}_{c}^{\top}\mathbf{G}_{p}\mathbf{L}(\delta)\mathbf{G}_{p}^{\top}\mathbf{Y}_{c}\}^{2}\{\mathbf{Y}_{c}^{\top}\mathbf{G}_{p}\mathbf{L}^{2}(\delta)\mathbf{G}_{p}^{\top}\mathbf{Y}_{c}\}^{\alpha/(1-\alpha)}}{\{\mathbf{Y}_{c}^{\top}\mathbf{G}_{p}\mathbf{L}(\delta)\mathbf{G}_{p}^{\top}\mathbf{G}_{p}\mathbf{L}(\delta)\mathbf{G}_{p}^{\top}\mathbf{Y}_{c}\}^{1-\{\alpha/(1-\alpha)\}}}$$

15: 
$$\delta_{p,\alpha} \leftarrow \arg\min_{\delta \in (-1,0) \cup (0,\infty)} - \ln Q(\delta)$$

16: 
$$\boldsymbol{b}_{p,\alpha} \leftarrow \mathbf{L}(\delta_{p,\alpha}) \mathbf{G}_p^{\top} \boldsymbol{Y}_{c} / \{ \boldsymbol{Y}_{c}^{\top} \mathbf{G}_{p} \mathbf{L}^{2}(\delta_{p,\alpha}) \mathbf{G}_{p}^{\top} \boldsymbol{Y}_{c} \}^{1/2}$$

17: 
$$\hat{w}_{p,\alpha} \leftarrow \boldsymbol{b}_{p,\alpha}^{\top} \mathbf{V}^{\top} \mathbf{W}^{-1/2} \boldsymbol{\psi}$$

18: **if** p = 1 **then** 

19: 
$$\hat{\beta}_{p,\alpha} \leftarrow N^{-1/2} (\boldsymbol{b}_{p,\alpha}^{\top} \mathbf{G}_{p}^{\top} \boldsymbol{Y}_{c}) (\boldsymbol{b}_{p,\alpha}^{\top} \mathbf{G}_{p}^{\top} \mathbf{G}_{p} \boldsymbol{b}_{p,\alpha})^{-1/2} \hat{w}_{p,\alpha}$$

20: else

21: 
$$\hat{\beta}_{p,\alpha} \leftarrow \hat{\beta}_{p-1,\alpha} + N^{-1/2} (\boldsymbol{b}_{p,\alpha}^{\top} \mathbf{G}_{p}^{\top} \boldsymbol{Y}_{c}) (\boldsymbol{b}_{p,\alpha}^{\top} \mathbf{G}_{p}^{\top} \mathbf{G}_{p} \boldsymbol{b}_{p,\alpha})^{-1/2} \hat{w}_{p,\alpha}$$

23: **for** 
$$i$$
 from 1 to  $N$  **do**

24: 
$$\int_{\mathcal{T}} \hat{\beta}_{p,\alpha} \hat{X}_{i} \leftarrow N^{-1/2} \left\{ \sum_{j=1}^{p} (\mathbf{b}_{j,\alpha}^{\top} \mathbf{G}_{j} Y_{c}) (\mathbf{b}_{j,\alpha}^{\top} \mathbf{G}_{j}^{\top} \mathbf{G}_{j} \mathbf{b}_{j,\alpha})^{-1/2} \mathbf{b}_{j,\alpha}^{\top} \mathbf{V}_{j}^{\top} \right\} \mathbf{W}^{1/2} \hat{c}_{i}$$

25: **end for**

26: 
$$\int_{\mathcal{T}} \hat{\beta}_{p,\alpha} \hat{\mu}_{[k]} \leftarrow \text{mean} \left\{ \int_{\mathcal{T}} \hat{\beta}_{p,\alpha} \hat{X}_{i} \mathbb{I} (X_{i} \in \Pi_{k}) : i = 1, \dots, N \right\}$$

27: 
$$\hat{\sigma}_{[k]}^{2} (\hat{\beta}_{p,\alpha}) \leftarrow \text{var} \left\{ \int_{\mathcal{T}} \hat{\beta}_{p,\alpha} \hat{X}_{i} \mathbb{I} (X_{i} \in \Pi_{k}) : i = 1, \dots, N \right\}$$

28: 
$$\hat{\sigma}_{pool}^{2} (\hat{\beta}_{p,\alpha}) \leftarrow (N-2)^{-1} \left\{ (N_{0}-1) \hat{\sigma}_{[0]}^{2} (\hat{\beta}_{p,\alpha}) + (N_{1}-1) \hat{\sigma}_{[1]}^{2} (\hat{\beta}_{p,\alpha}) \right\}$$

29: **for**  $i$  from 1 to  $N$  **do**

30: 
$$\hat{\mathcal{D}}_{Q} (\hat{X}_{i} \mid \hat{\beta}_{p,\alpha}) \leftarrow \hat{\sigma}_{[1]}^{-2} (\hat{\beta}_{p,\alpha}) (\int_{\mathcal{T}} \hat{\beta}_{p,\alpha} \hat{X}_{i} - \int_{\mathcal{T}} \hat{\beta}_{p,\alpha} \hat{\mu}_{[1]})^{2}$$

31: 
$$-\hat{\sigma}_{[0]}^{-2} (\hat{\beta}_{p,\alpha}) (\int_{\mathcal{T}} \hat{\beta}_{p,\alpha} \hat{X}_{i} - \int_{\mathcal{T}} \hat{\beta}_{p,\alpha} \hat{\mu}_{[0]})^{2} + 2 \ln \frac{N_{0}\hat{\sigma}_{[1]}(\hat{\beta}_{p,\alpha})}{N_{1}\hat{\sigma}_{[0]}(\hat{\beta}_{p,\alpha})}$$

32: 
$$\hat{\mathcal{D}}_{L} (\hat{X}_{i} \mid \hat{\beta}_{p,\alpha}) \leftarrow \hat{\sigma}_{pool}^{-2} (\hat{\beta}_{p,\alpha}) (\int_{\mathcal{T}} \hat{\beta}_{p,\alpha} \hat{X}_{i} - \int_{\mathcal{T}} \hat{\beta}_{p,\alpha} \hat{\mu}_{[0]})^{2} + 2 \ln (N_{0}/N_{1})$$

34: **end for**

35: **end for**

36: 
$$\mathbf{GCV}(p,\alpha) \leftarrow \sum_{i=1}^{N} [Y_{i} - \mathbb{I} \{\hat{\mathcal{D}}_{Q} (\hat{X}_{i} \mid \hat{\beta}_{p,\alpha}) < 0\}]^{2} / (N-p-2)^{2}$$

37: 
$$\mathbf{or} \sum_{i=1}^{N} [Y_{i} - \mathbb{I} \{\hat{\mathcal{D}}_{L} (\hat{X}_{i} \mid \hat{\beta}_{p,\alpha}) < 0\}]^{2} / (N-p-2)^{2}$$

38: **end for**

39:  $(p_{\text{opt}}, \alpha_{\text{opt}}) \leftarrow \arg\min_{(p,\alpha)} \text{GCV}(p,\alpha)$